CO_2 Injection in Vertical and Horizontal Cores: Measurements and Numerical Simulation

Joachim Moortgat, Abbas Firoozabadi, and **Zhidong Li,** RERI; and **Rogério Espósito,** Petrobras

Summary

In certain high-pressure and low-temperature reservoirs, the density of CO_2 may be substantially higher than the oil density. Upon mixing of CO_2 and oil, a gas phase with a high content of methane (C_1) may also appear. When the C_1 content is high, this gas phase may have a lower density than the oil. In relation to this phenomenon, we have conducted three comprehensive experiments studying CO_2 injection from the top and bottom of a vertical core and injection in a horizontal core. The injection rate is 1 PV/day. This low rate allows the study of diffusion. The core diameter used in this work is 3.8 cm and the length is 27.3 cm. The tests are conducted at a pressure of 441 bar and a temperature of 60°C. At 2.6 hydrocarbon pore volume injection (PVI), the coreflood results give a recovery of 98% for bottom injection, 84% for top injection, and 92% for horizontal injection. We have also conducted an extensive set of measurements to determine swelling, viscosity, and density for the calibration of an equation of state. We simulate the experiments using a state-of-the-art higher-order finite-element three-phase compositional model. The simulations suggest that the endpoint relative permeability of the CO_2-rich phase may be lower than the oil phase. The results also show that Fickian diffusion should be taken into account, but that the diffusion coefficients are reduced, because the CO_2/oil mixtures are in the near-critical region for much of the injection. Even for a horizontal core there is a considerable gravity effect. One main conclusion is that there may be vast differences between CO_2 injection in a 1D slim tube and in a core where there may be a 2D flow. A related conclusion is that analysis of CO_2 coreflooding may provide important parameters for field-scale problems.

Introduction

CO_2 injection is being increasingly considered to improve oil recovery in both new reservoirs, and reservoirs that have been previously depleted and/or water flooded (DOE 2011). Compared with water and nitrogen injection, CO_2 injection may offer important advantages because of strong phase behavior:

1. When CO_2 dissolves in oil, it may increase the liquid volume (swelling), expelling oil from the rock matrix. This is a large-scale effect: when the oil volume increases in the CO_2-invaded region, it forces the oil to flow throughout the domain. Swelling may also increase oil recovery beyond the residual oil saturation: when CO_2 dissolves in the "residual" oil, it may increase the oil volume above the residual saturation, allowing more oil to flow.

2. Residual oil may evaporate when exposed to a sufficient flow of CO_2-rich gas. Because of evaporation, the concept of residual oil may not be relevant when studying CO_2 injection.

3. When CO_2 mixes with oil, it may reduce the oil viscosity and increase the fluid mobility. This, however, is a local effect. Furthermore, the opposite may also happen: lighter components may evaporate and be flushed out, leaving a denser, more viscous oil.

4. The high solubility of CO_2 in oil significantly reduces the effect of capillary pressure in studying CO_2 injection, in particular at high reservoir pressures (Firoozabadi et al. 1988). In this work, we will neglect capillarity.

5. We demonstrate in this work that CO_2 injection may alter the rock wettability and result in a low-endpoint, CO_2-rich gas relative permeability.

6. Finally, a unique phase-behavior effect of CO_2-oil mixing is that the density of the oil may increase because of the CO_2 dissolution (Simon et al. 1978; Ashcroft and Isa 1997). This may either aid gravitational drainage or potentially make the front gravitationally unstable, as we will discuss in this paper.

In addition to improved oil recovery, there is the environmental and economic interest in using CO_2 injection in depleted reservoirs to store CO_2 from industrial sources in order to alleviate the effect of CO_2 emission on global warming.

The unique phase behavior mentioned previously makes CO_2 injection a desirable option for enhanced oil recovery (EOR). At the same time, successful CO_2-injection projects require a better understanding of the process. Given the exceedingly large scale of field problems and cost of pilot projects, it is illustrative to study specific aspects of the CO_2 injection process in laboratory experiments. In this paper, we will consider gravitational effects by positioning a core either in a horizontal or a vertical position. In the latter case, we will compare CO_2 injection from the bottom and from the top. Because the CO_2 density is higher than the oil density for the conditions of our interest, injection from the top is expected to be gravitationally unstable without significant Fickian diffusion. In the experiments and subsequent modeling, we study the effects of the instability on breakthrough, recovery, and composition in the production stream.

In the literature, and in most commercial simulators, Fickian diffusion is neglected and assumed to be unimportant in homogeneous media where significant compositional gradients only occur near the front. In this work, we find that when Fickian diffusion is neglected altogether, there is no restoring force at the onset of the gravitational instability. Small perturbations therefore grow into large-scale gravitational fingers and fast natural convection (Rongy et al. 2012). Diffusion may dampen these instabilities, with consequences for breakthrough times and final recovery. For the experiments considered in this work, the mixtures of CO_2 with oil turn out to be in the near-critical region, where the diffusion coefficients are reduced and the diffusive restoring force is weaker than at conditions far from the critical point.

To model the experiments, we use our three-phase compositional simulator (Moortgat et al. 2011, 2012), which uses higher-order discontinuous Galerkin (DG) methods to explicitly update mass transport (compositions) and the mixed hybrid finite-element (MHFE) model to implicitly solve for the pressure and velocity fields simultaneously and to the same order of accuracy (Hoteit and Firoozabadi 2005, 2006a,b). Multicomponent Fickian diffusion coefficients are derived from irreversible thermodynamics (Leahy-Dios and Firoozabadi 2007) and diffusion phase fluxes are weighed by their saturations (Moortgat and Firoozabadi 2010) and reduced by the porosity. The MHFE model provides accurate continuous velocity fields, while the DG treatment of mass transport guarantees higher-order accurate compositions. This accuracy is required to capture the small scales at which gravitational

This paper (SPE 135563) was accepted for presentation at the SPE Annual Technical Conference and Exhibition, New Orleans, 4–7 October 2009, and revised for publication. Original manuscript received for review 2 May 2011. Revised manuscript received for review 1 November 2011. Paper peer approved 28 March 2012.

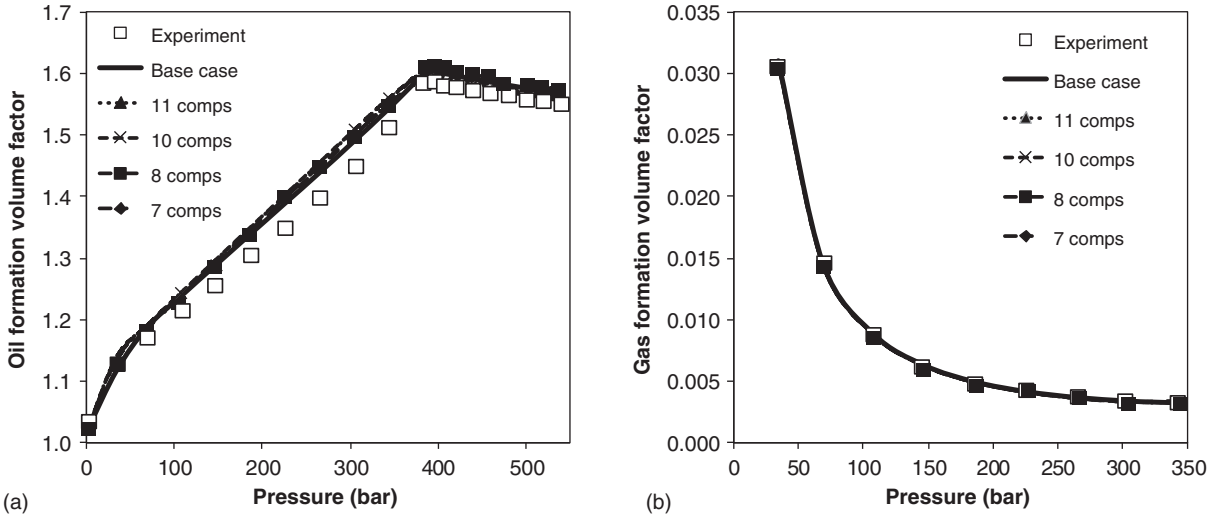

Fig. 1—(a) Oil and (b) gas formation volume factor vs. pressure at 331.85 K.

fingers and convective eddies may occur when the front becomes gravitationally unstable. Lower-order finite difference (FD) methods may obscure even laboratory scale fingers because of the high numerical dispersion.

Injection of supercritical CO_2, that is denser than oil is of interest in enhancing oil recovery from some of the world's largest oil reservoirs. Yet no comprehensive laboratory experiments have been carried out to study the associated gravitational effects that may impact flow paths and recovery. In this work, we aim to carry out such an investigation. To understand the main physical processes, and to generalize to larger scales, we need reliable numerical modeling. Currently available simulators do not incorporate fully compositional three-phase flow, which satisfies thermodynamic equilibrium by requiring the species' fugacities to be equal in all three phases, nor do they use an accurate equation of state (EOS) for the aqueous phase. More importantly, commonly used FD methods suffer from numerical dispersion, which may mask the gravitational and viscous instabilities that are the main subject of this investigation. Instead, we employ higher-order finite-element methods for increased accuracy, a fully compositional three-phase split computation, and an accurate cubic-plus-association EOS for the aqueous phase. The oil and gas phase properties are modeled with the Peng-Robinson (PR) EOS (Peng and Robinson 1976). Another focus of the work is a careful examination of relative permeabilities because CO_2 injection may result in significant wettability alteration and a low-endpoint gas relative permeability.

This paper is organized as follows: first, we briefly discuss our modeling of PVT experiments of differential liberation, including fluid characterization and parameter adjustment of an EOS, to accurately calculate the oil's physical properties and phase behavior. In the second part of the paper, we describe the three CO_2 injection experiments (horizontal injection and vertical injection from the top and bottom), summarize our numerical model, and present our simulation results. We end with our main conclusions.

PVT Data and Modeling

We have measured the oil volume, solution gas/oil ratio (GOR), oil viscosity, and gas formation volume factor of the reservoir oil as a function of pressure at a reservoir temperature of 331.9 K in differential liberation. We have also measured the bubblepoint pressure and oil swelling as a function of dissolution of CO_2, increasing the molar fraction of mixed CO_2 to approximately 35 mol%. We adopt the PR-EOS with volume translation (Jhaveri and Youngren 1988) for the hydrocarbon phases and the cubic-plus-association and cross-association EOS (Li and Firoozabadi 2012) for the aqueous phase.

The PVT measurements were first matched by a full fluid description of pure components up to a residue of C_{30+}. To facilitate efficient compositional simulation of the experiments, we considered various lumping choices, ranging from 6 to 11 (pseudo-) components, and with residues of C_{20+}, C_{25+}, or C_{30+}. We find that extraction by CO_2 of heavier components (above C_{20}) may be captured with sufficient accuracy by a residue of C_{20+} and find no improvement from additional pseudocomponents in the C_{20}–C_{30} range. The most computationally efficient characterization that accurately reproduces the experimental data has nine components and a residue of C_{20+}. Details of the tuned fluid model are given in the Appendix.

Instead of the Lohrenz-Bray-Clark (LBC) model (Lohrenz et al. 1964), we use the Christensen and Pedersen (2006) model (CP) to correlate and predict the phase viscosities in both PVT and coreflooding experiments. The CP model is based on the corresponding-state principle and shows much better performance than the LBC model to correlate the oil viscosity in the PVT experiments. More importantly, the CP model uses a unified approach for the gas and oil phases. This is attractive for our purpose because the coreflooding experiments are conducted in the critical region where the two equilibrium phases are nearly indistinguishable. The CP model has two adjustable parameters.

In the PVT experiments, because the conditions are far from the critical point, the volume translation is applied to the oil phase only, as in the conventional three-parameter PR-EOS. However, in simulating the coreflooding experiments, the volume translation is applied to both the oil and gas phases and smaller CO_2-related BICs (0.08) are used to match the data because the conditions are in the critical region. By using the CP model and applying a volume shift to both phases, both viscosities and densities are continuous across the critical region and insensitive to phase identification.

Figs. 1 through 3 present the comparison between measurements and calculations for the differential liberation. Computed values are given for both the base-case nine-component pseudoization up to C_{20+} and four pseudoizations up to C_{30+} with 7, 8, 10, and 11 (pseudo-) components (see the Appendix). When the pressure is higher than the bubblepoint, the mixture is in single-phase state. As the pressure increases, the oil volume slightly decreases (Fig. 1a), the oil viscosity and density slightly increase (Fig. 2), and the GOR is constant (Fig. 3). When the pressure is lower than the bubblepoint, the mixture is in two-phase state. As the pressure is decreased, the gas phase is removed in each liberation step, resulting in a steep decrease in the oil volume and GOR. At the same time, the oil viscosity and density increase significantly owing to the evaporation of the light components. Our calculations agree well with the experiments. Note in Fig. 2b that the CP model correlates better with the experimental viscosity data than does the LBC model, as mentioned previously. In **Fig. 4,** we compare the data with our calculations of CO_2 mixing. The data

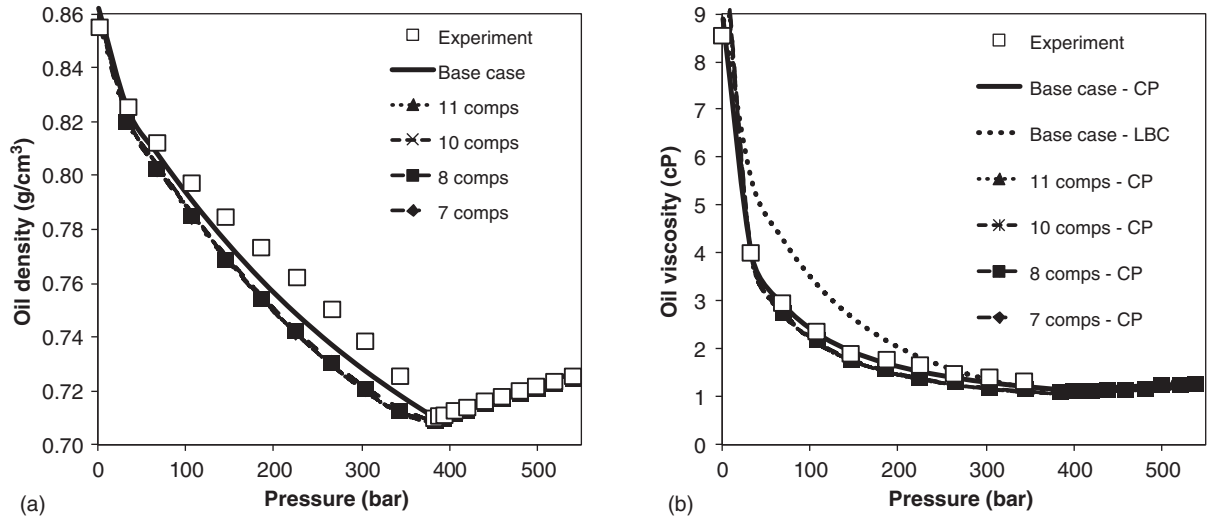

Fig. 2—(a) Oil density and (b) viscosity vs. pressure at 331.85K for the differential liberation experiment.

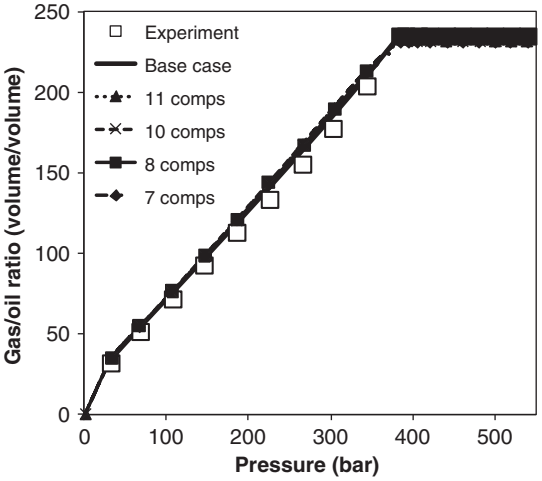

Fig. 3—GOR vs. pressure at 331.85 K, both at standard condition.

of bubblepoint pressure at 28 and 35.5 mol% of injected CO_2 show relatively high uncertainty. Again, we accurately reproduce the increase of the bubblepoint pressure and the swelling of the volume caused by CO_2 dissolution. The predictions from the five different fluid characterizations show comparable accuracy, with the best agreement achieved by the nine-component base-case characterization up to C_{20+}, in particular for oil density and viscosity.

Core Injection Experiments and Simulation

In the previous section, we characterized the reservoir oil and obtained the EOS parameters to predict the fluid-phase behavior. In this section, we will consider three CO_2 injection experiments and their numerical modeling. First, we will describe the experiments, then provide a brief description of our three-phase compositional algorithm, and finally discuss our modeling of the experiments and further interpret the results.

Coreflood Experiments. Three CO_2 injection tests are conducted in the same sandstone core from the side in a horizontal core and from the top and bottom in a vertical core. The core has a length $L = 27.3$ cm, and radius $R = 1.9$ cm.

First, the core was water-saturated. An effective permeability to water of 451 md was measured once at the beginning of the corefloods. The horizontal coreflood was run first. Live oil was used to displace the water and age the core for 4 weeks. After aging, more than 10 PV of live oil was injected until the GOR was stable and there was no more water production. Three

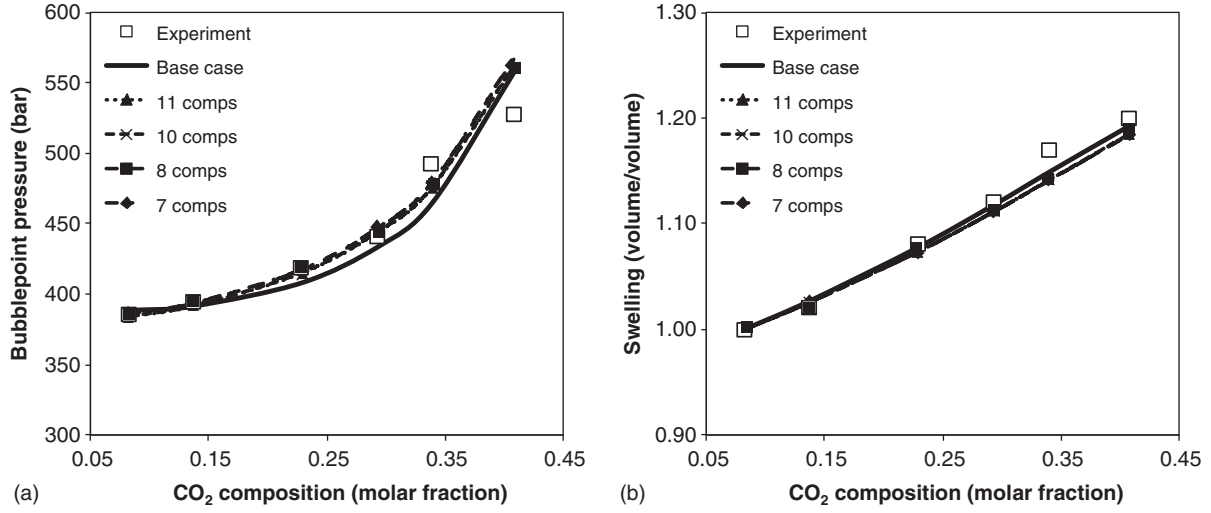

Fig. 4—(a) Bubblepoint pressure and (b) swelling of the oil vs. dissolved CO_2 (molar fraction) at 331.85 K.

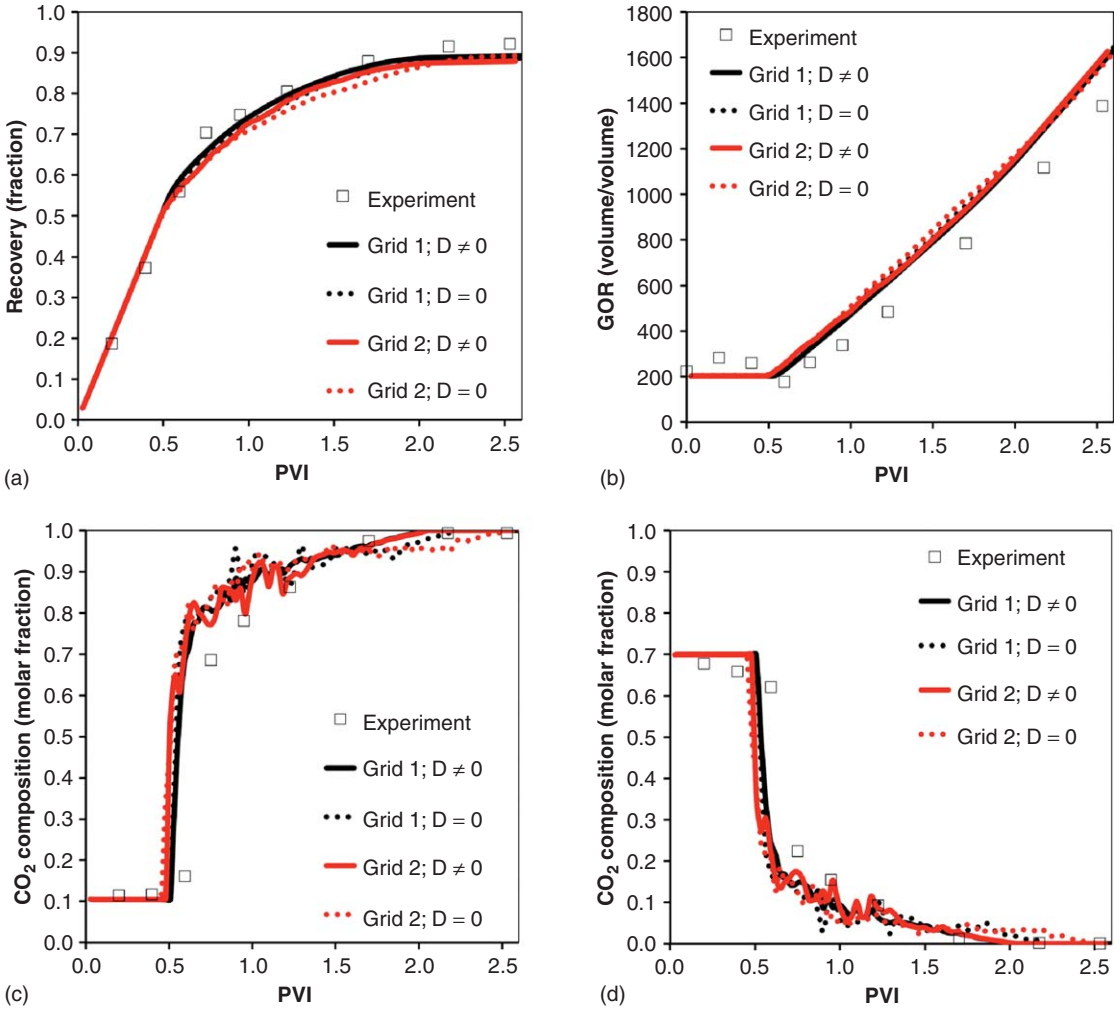

Fig. 5—Experiment 1: Measured data and simulation results with Fickian diffusion (denoted as D ≠ 0) and without Fickian diffusion (D = 0) for (a) oil recovery, (b) GOR, and (c) CO_2 and (d) C_1 composition in the gas phase of production stream flashed to surface conditions. DG computations on 100×21 element grid (Grid 1) and 250×50 grid (Grid 2).

different injection rates were used to measure an effective permeability to oil of 221 md. The porosity is 18.8%.

To recondition the core for the second and third (vertical) coreflloods, we injected live oil to displace CO_2 for more than 10 PV and we measured the effective permeability. The measured oil permeabilities and connate water saturation of 31% were within the experimental error for the three experiments. The purpose of the experiments in this paper is to investigate and simulate CO_2 floods under the effect of orientation. For the sake of consistency, we have used the same values for absolute and relative permeabilities in the modeling of all three experiments.

Both in the restoration process and in all coreflooding tests, the temperature is $T = 331.2$ K and the confining pressure is $p = 648.1$ bar. CO_2 is injected at a rate of one hydrocarbon PV per day. Note that the core PV is 58 cm^3 and the hydrocarbon PV is 40 cm^3. In all three experiments, the outlet pressure is kept constant at $p = 441.3$ bar and the pressure drop across the core is less than 0.034 bar.

In the three tests, we measure the oil recovery, GOR, and the composition of the produced fluid at the outlet. The measured, as well as simulated, results are summarized in **Figs. 5 through 7.** In the following, we discuss the essence of the measurements, and later we will provide further discussion in the simulations section.

Experiment 1: CO_2 Injection in the Horizontal Core. Fig. 5a shows the recovery data vs. PV of injected CO_2 in the horizontal core. The recovery plot indicates a final recovery of around 92%, which is somewhere between the bottom and top injection in the vertical core, to be discussed shortly. As we will see in the simulation section, the large density difference of 0.18 g/cm^3 between injected CO_2 and oil-in-place results in a substantial gravity effect even in the horizontal core.

Experiment 2: CO_2 Injection in the Top. Fig. 6a shows a recovery of approximately 83% from CO_2 injection from the top in the vertical core. Because of the high density of CO_2 of 0.92 g/cm^3, and an oil density of 0.74 g/cm^3, we expect an unstable front, provided it is not stabilized by Fickian diffusion. This aspect of flow will be discussed in detail in the simulation section.

Experiment 3: CO_2 Injection in the Bottom. As Fig. 7a shows, bottom injection of CO_2 achieves the highest recovery of 98% of the initial oil-in-place. Only if mixing of CO_2 with the oil results in a methane-rich gas might the front be unstable because of the lower local density of the gas phase. Otherwise, the displacement is stable and efficient.

Compositional Modeling Algorithm. We model the experiments with our three-phase compositional modeling code, which is based on an implicit-pressure, explicit-composition scheme that uses higher-order finite-element methods. The pressure equation and the Darcy relation for the sum of the phase fluxes are solved implicitly using the MHFE method, while the mass-transport equation is solved explicitly by the DG approach. Details of the basic algorithm, as applied to two-phase flow, can be found in Hoteit and Firoozabadi (2005, 2006a,b, 2009), Moortgat and Firoozabadi (2010), and the generalization to three-phase flow in Moortgat et al. (2011, 2012). The merit of this approach is that

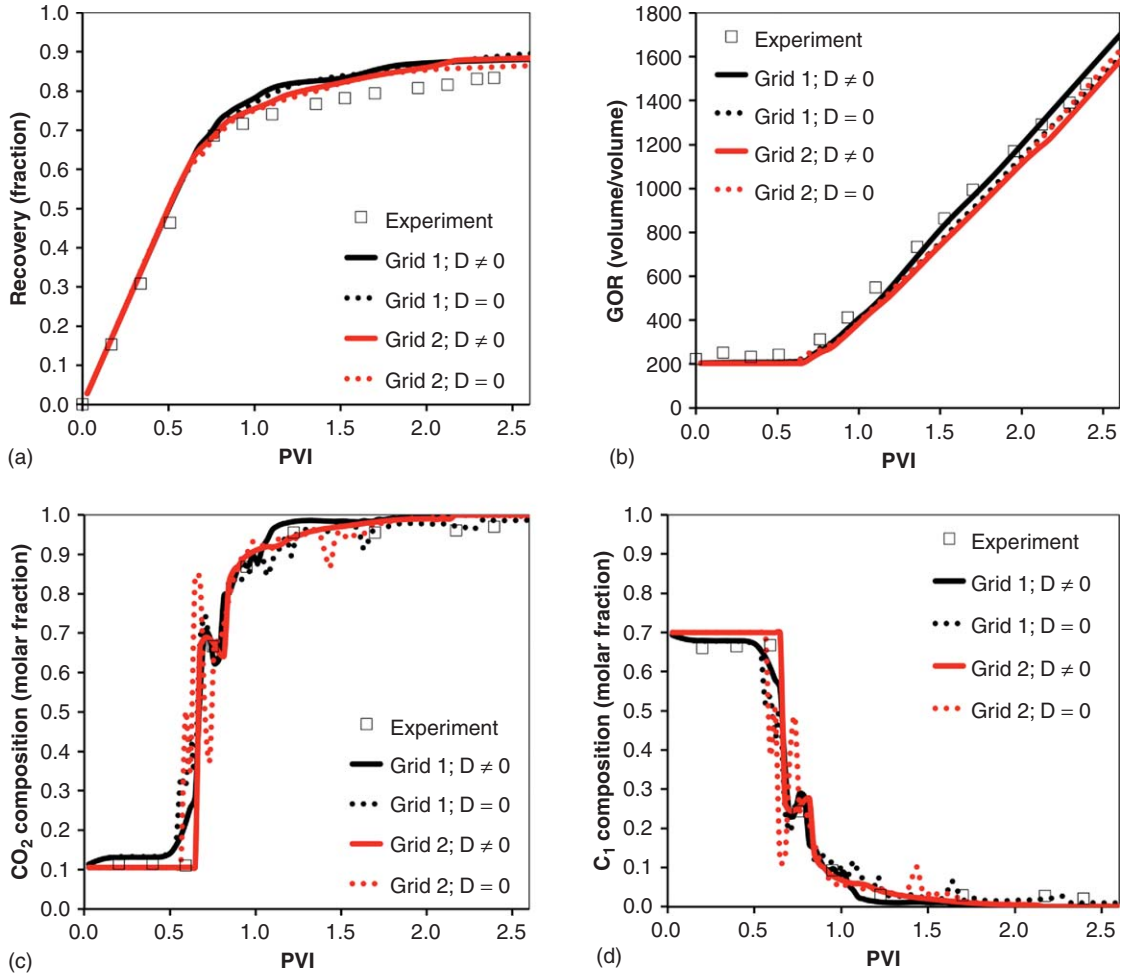

Fig. 6—Experiment 2: Measured data and simulation results with (D ≠ 0) and without (D = 0) Fickian diffusion for (a) oil recovery, (b) GOR, and (c) CO_2 and (d) C_1 composition in the gas phase of production stream flashed to surface conditions. Results computed using bilinear DG on 100×21 element grid (Grid 1) and 250×50 element grid (Grid 2).

the pressure and velocity fields are obtained simultaneously and to the same order of convergence. Also, mass transport is calculated at a higher-order accuracy, which results in low numerical dispersion and grid-orientation effects. To obtain a comparable accuracy using finite-difference methods requires significantly finer grids and higher CPU times.

We account for compressibility, gravity, Fickian diffusion, phase-behavior effects, and viscous forces. In the near-critical region, the fluid mixtures exhibit various unusual properties that comprise the bulk of this study. Exceedingly robust and accurate phase-splitting algorithms are required. For the aqueous phase, we assume that the mutual solubility of water and hydrocarbons is negligible. Only CO_2 dissolves in water and water does not evaporate (this assumption is satisfied for $T = 331$ K). The CO_2 composition in the aqueous phase, as well as in the oil and gas phases, is computed by requiring the equality of fugacities in all three phases. This is an improvement over Henry's law, which cannot strictly satisfy the equality of fugacities in a multicomponent three-phase mixture, and therefore violates thermodynamic equilibrium.

Our treatment of Fickian diffusion (Moortgat and Firoozabadi 2010) for the hydrocarbon phases is based on the work by Leahy-Dios and Firoozabadi (2007), while diffusion is neglected within the connate water. Leahy-Dios and Firoozabadi (2007) compute the full matrix of multicomponent diffusion coefficients from irreversible thermodynamics considerations in combination with a correlation for the infinite dilution diffusion coefficients. The infinite dilution diffusion coefficients are the binary diffusion coefficients for a two-component system in which one of the components is infinitely diluted in the other component. To obtain the diffusive fluxes in each phase, the fluxes are weighted by the phase saturations.

In porous media, the diffusion coefficients are lower than in open space because of porosity and tortuosity. The reduction factor (or diffusivity) is commonly assumed to be of the form, ϕ/τ, where ϕ is the porosity and τ the tortuosity, which is of the order 1 to 6 (Brigham et al. 1961; Donaldson et al. 1976; Cussler 1997). There does not seem to be a consensus in the literature on the exact functional form of the diffusivity factor. Empirical or semi-empirical correlations may disagree with theoretical relations, which are generally derived from idealized pore models packed with spherical or tetrahedral material. Van Brakel and Heertjes (1974) provide a review of various dependencies on porosity and tortuosity. Given this uncertainty, the diffusion coefficients may have to be reduced by as much as an order of magnitude from the open space values.

Furthermore, Fickian diffusion coefficients and fluxes in the critical region need careful consideration. On the basis of thermodynamic stability analysis, the matrix of Fickian diffusion coefficients reduces to zero as the critical point is approached (Ghorayeb and Firoozabadi 2000). There is also clustering of molecules in the critical region, which may result in significant reduction of the Fickian diffusion coefficients (Cussler 1997). To account for these various effects, we have seen a need to decrease diffusion coefficients by a constant overall factor of 0.01 in this work.

In the near-critical region, the gas and liquid phases have similar properties and mix efficiently, which can be modeled by a linear relative permeability model. From the 98% recovery in Experiment 3, we conclude that there is essentially no residual oil

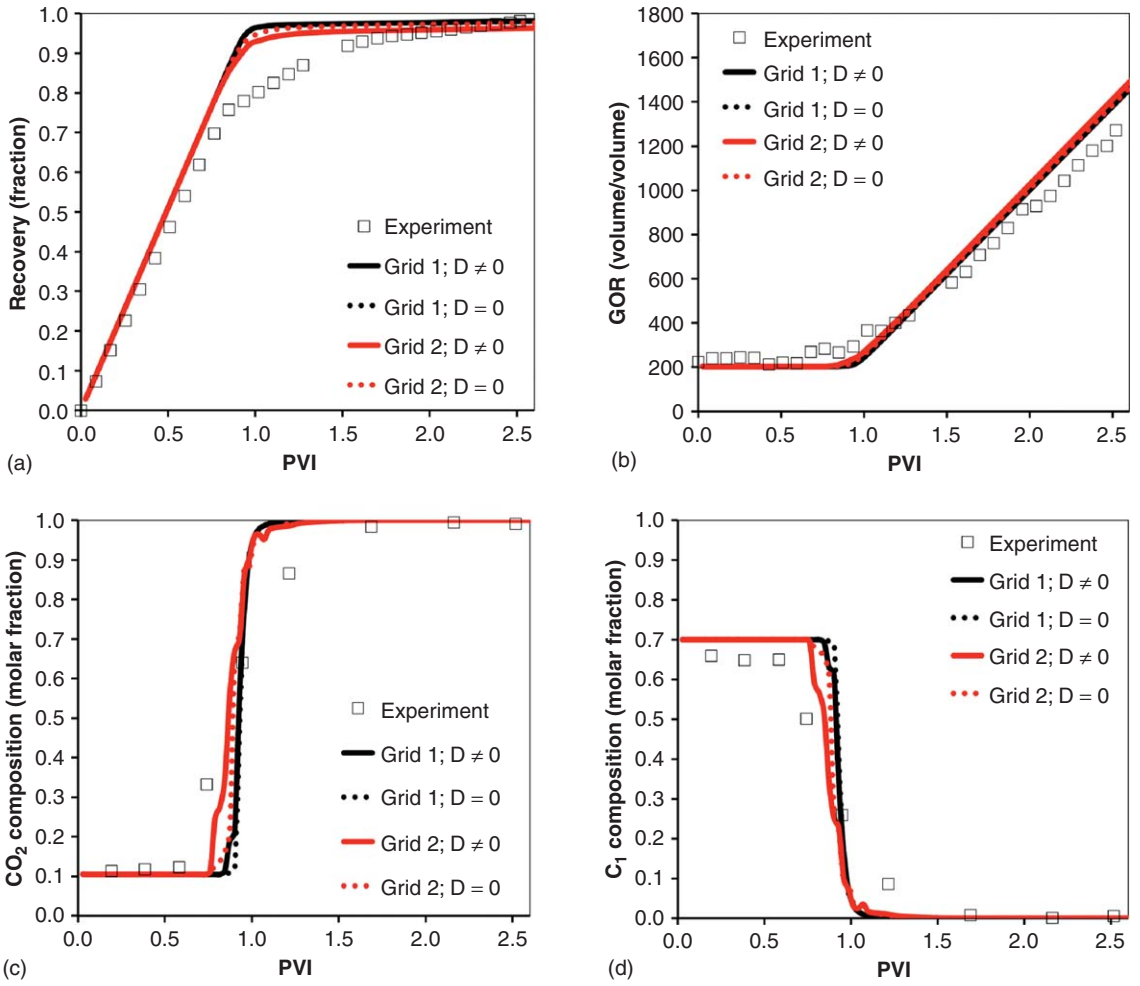

Fig. 7—Experiment 3: Measured data and simulation results with (D ≠ 0) and without (D = 0) Fickian diffusion for (a) oil recovery, (b) GOR, and (c) CO_2 and (d) C_1 composition in the gas phase of production stream flashed to surface conditions. Results computed using bilinear DG on 100×21 element grid (Grid 1) and 250×50 element grid (Grid 2).

saturation to CO_2 injection. An unusual property of CO_2 is that it may alter the wettability of rock and may have an endpoint relative permeability lower than that of the oil. In the modeling of all three experiments, we find gas and oil relative permeability endpoints of $k^0_{rg} = 0.4$ and $k^0_{ro} = 0.6$, respectively. We discuss the effect of alternative relative permeability relations in the following.

The effect of capillary pressure in the high-pressure gas/oil flow is negligible because of a low interfacial tension. At the bubblepoint pressure, various mixtures of CO_2 with the initial oil give a low (computed) interfacial tension, as shown in **Fig. 8.** For comparison, the interfacial tension of a CO_2/water mixture at the conditions of the experiment ($p = 441.3$ bar, $T = 331.2$ K) is approximately 20 mN/m. We will therefore neglect capillarity in the discussion of numerical modeling that follows.

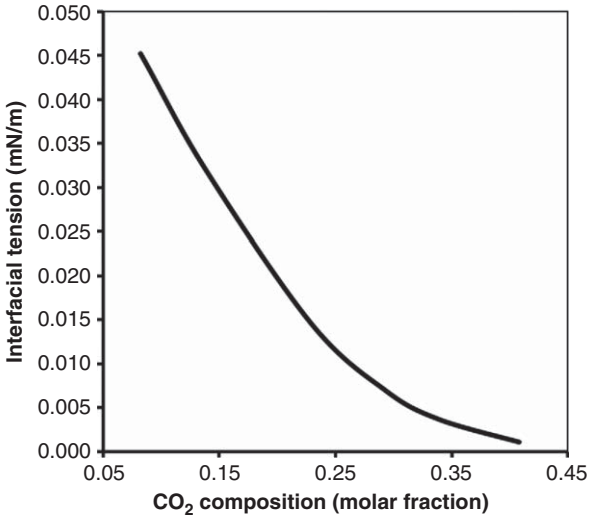

Fig. 8—Computed interfacial tension vs. dissolved CO_2 (molar fraction) at 331.85 K and at the bubblepoint pressures from Fig. 4a.

Simulation Results. In the following subsections, we will discuss our modeling of the three experiments. To understand specific factors affecting the efficiency of CO_2 injection for EOR, we isolate the essential effects of gravity and diffusion. The former is by experimental design, assuming that the effect of gravity is more pronounced in a vertical than a horizontal core (although we will see that gravity may also influence horizontal injection). The latter we investigate numerically by performing simulations of the experiments with and without accounting for Fickian diffusion. Numerical dispersion will mask some of these aspects when either the mesh is insufficiently refined or, equivalently, lower-order methods are used (such as finite difference). We will provide an example of the latter for Experiment 2.

To model the experiments with our 2D compositional model, we take a diametrical cross section of the core with rectangular dimensions of 27.3×3.8 cm^2 (with the long side in either the horizontal or vertical direction). The horizontal experiment is modeled on a 100×21 element mesh. For the vertical experiments, we

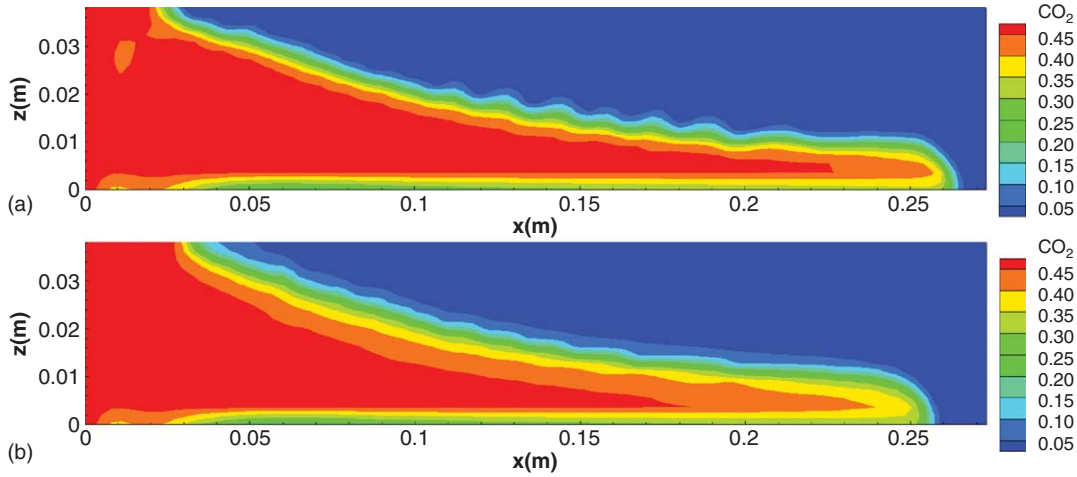

Fig. 9—DG simulations of Experiment 1: Overall CO_2 composition (molar fraction) at 0.45 PVI (a) without and (b) with Fickian diffusion on 100×21 mesh.

use a 20×100 mesh. We refer to the coarse meshes as Grid 1 in the figures. We verify the convergence of the results in Figs. 5 through 7 by repeating the simulations on a 250×50 (or 50×250) element mesh, referred to as Grid 2. All the simulations on Grid 1 were also repeated with the seven- and 10-component pseudoizations with residue C_{30+} discussed in the Appendix and included in Figs. 1 through 4. The simulation results are nearly identical, and not shown for brevity. Finally, we investigate the effect of small heterogeneities in the rock cores by performing additional simulations (discussed next), in which the permeability in each grid cell is randomly perturbed by 5% around the average permeability, using the Fortran random-number generator. The core was visually examined and does not suggest large heterogeneities.

Because of connate water, the hydrocarbon pore volume (denoted as PV) in the cross-section is 13.5 cm^2. We choose the injection rate as 1 PV/day with respect to this volume. The rock porosity is 18.8%, and the hydrocarbon porosity is 13.0%. At the injection end of the core, we distribute injection wells over all mesh elements on that domain boundary. At the production end, we consider a single production element, where the pressure is kept at a constant $p = 441.3$ bar. The isothermal temperature is $T = 331.2$ K.

Experiment 1: CO_2 Injection in the Horizontal Core. When CO_2 is injected in the horizontal core, we find that the effect of gravity is significant, even though the diameter is relatively small compared to the horizontal length. **Fig. 9** shows results for simulations without and with accounting for Fickian diffusion on Grid 1 at 45% hydrocarbon PVI (note that in this and all similar figures, the x- and z- axis have independent scales). The denser CO_2 initially flows underneath the lighter oil, resulting in relatively early breakthrough. After breakthrough, the recovery rate is reduced (Fig. 5a) because of gas production, and the GOR increases (Fig. 5b). The breakthrough time can be seen most clearly in the compositions in the production well. Figs. 5c through 5d show the CO_2 and C_1 compositions, respectively, in the gas phase of the production stream after flashing to surface conditions.

Fig. 9a shows the appearance of small-scale gravitational plumes, which are resolved more clearly on Grid 2 in **Fig. 10.** At the interface between oil and CO_2-rich gas, methane evaporates into the gas phase, which results in a mixture that is lighter than the oil and the dense CO_2. This lighter gas buoyantly rises upward. Even the small degree of Fickian diffusion in Figs. 9b and 10b largely suppresses the gravitational instability. Numerical dispersion in lower-order methods further suppresses this instability. However, in this experiment, the flow is predominantly in the horizontal direction and we find that the small extent of vertical gravitational fingering does not significantly affect the flow. Results from finite difference simulations with and without Fickian diffusion are comparable (not shown). The effect of diffusion is mostly seen in smearing out some of the fluctuations in the compositions in the production well, observed in the simulations without diffusion (Figs. 5a and b). In field-scale problems and at low injection rates, the gravitational fingering may have more significant effect and numerical dispersion needs to be reduced further. The panels

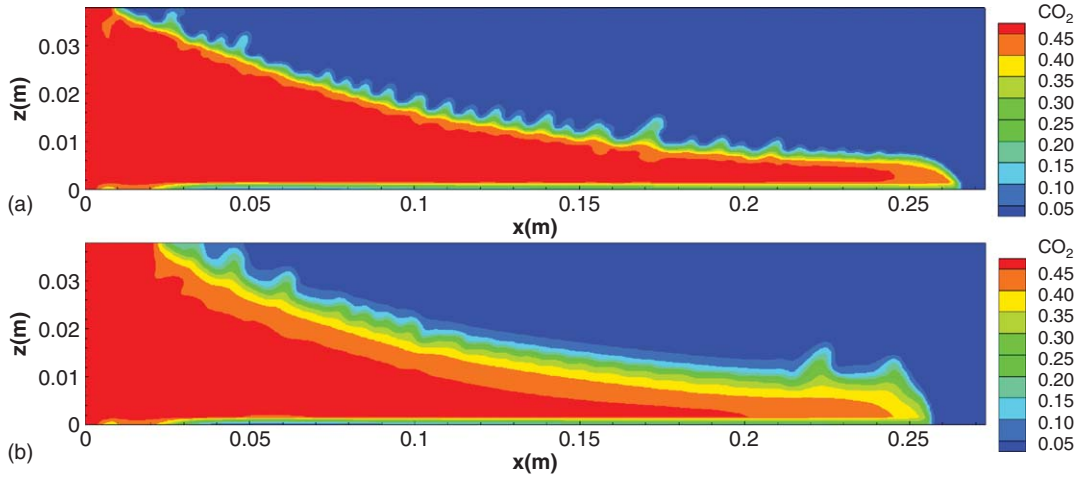

Fig. 10—DG simulations of Experiment 1: Overall CO_2 composition (molar fraction) at 0.45 PVI, (a) without and (b) with Fickian diffusion on 250×50 mesh.

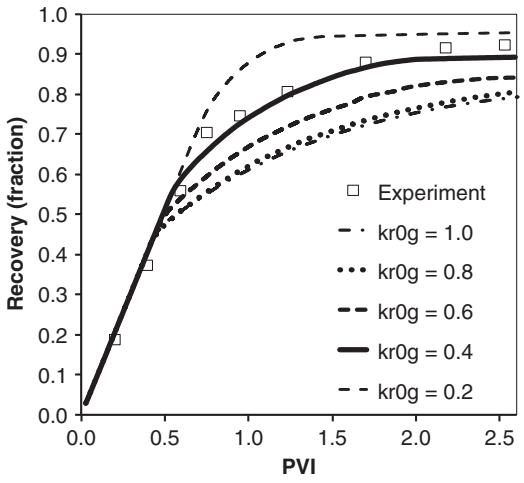

Fig. 11—DG simulations of Experiment 1: Dependence of oil recovery on endpoint relative permeability for gas phase, computed on 100×21 mesh with Fickian diffusion.

in Fig. 5 show that the simulation results have essentially converged on the coarse Grid 1 in terms of production data.

Apart from the effects of gravity and diffusion, these experiments provide insights in the relative permeability pertaining to CO_2 injection. We carried out an extensive parameter study, varying the exponents and endpoint relative permeabilities of the oil and gas phases. We find that the results are insensitive to the exponents and the endpoint oil relative permeability, but are sensitive to the endpoint gas relative permeability. **Fig. 11** shows the impact on recovery for a number of simulations (on Grid 1) in which the gas endpoint relative permeability is varied with respect to the base case of $k^0_{rg} = 0.4$, while the other parameters are kept the same. These findings are reasonable: there is a relatively sharp transition from a nearly single-phase gas region to a single-phase oil region (excluding the connate water). In these regions, the relative permeabilities are near their respective endpoint values. The endpoint gas permeability therefore strongly determines the gas mobility and hence the breakthrough time. More interestingly, the experimental results suggest that the CO_2-rich gas phase may have a lower endpoint than the oil, and behaves as the intermediate wetting phase. This finding is in line with some of the data in Müller (2011) for both CO_2/water and CO_2/oil systems. As a final note, a gas endpoint of $k^0_{rg} = 0.3$ (rather than $k^0_{rg} = 0.4$) results in a slightly later breakthrough time for this experiment, and better reproduces the measured GOR and compositions in the production well. However, $k^0_{rg} = 0.4$ provides the best self-consistent agreement with the measured data across all three experiments, as we will illustrate in the following.

Two more simulations (with and without Fickian diffusion) were performed on Grid 1, in which a 5% heterogeneous spread in rock permeability was introduced, as mentioned previously. The heterogeneities result in slightly different arrival times of the gravitational fingers and plumes, observed in Figs. 5c, 5d, 9, and 10. The recovery and GOR, however, are indistinguishable from the simulations for a homogeneous permeability (not shown).

Experiment 2: CO_2 Injection From the Top. In the second experiment, the core is placed in the vertical position, and CO_2 is injected from the top. Because the CO_2 is denser than the oil, the flow is gravitationally unstable. When Fickian diffusion is neglected or is weak near the critical region, there is no stabilizing force and the instability develops at an early time. Initially, the denser CO_2 starts to "droop" in the form of gravitational fingers. Next, when density gradients develop at an angle to the pressure gradients, this is a source term for vorticity in the velocity field, which manifests itself as natural convection. Because of convection, there is not only downward gravitational drainage, but also flow in the horizontal and upward directions. Upward flow may also be induced by evaporation of methane into the CO_2-rich gas phase, resulting in gravitational plumes of lighter gas.

Fig. 12 shows the overall CO_2 composition throughout the domain around the time of breakthrough (0.67 PVI) for simulations with and without Fickian diffusion, and on both Grid 1 and Grid 2. Some smaller-scale features are resolved on Grid 2. However, despite the chaotic small-scale flow, the results converge quite well in terms of breakthrough time, recovery, GOR, and compositions in the production well, as shown in Fig. 6. Comparing the results with and without diffusion, we see that diffusion stabilizes

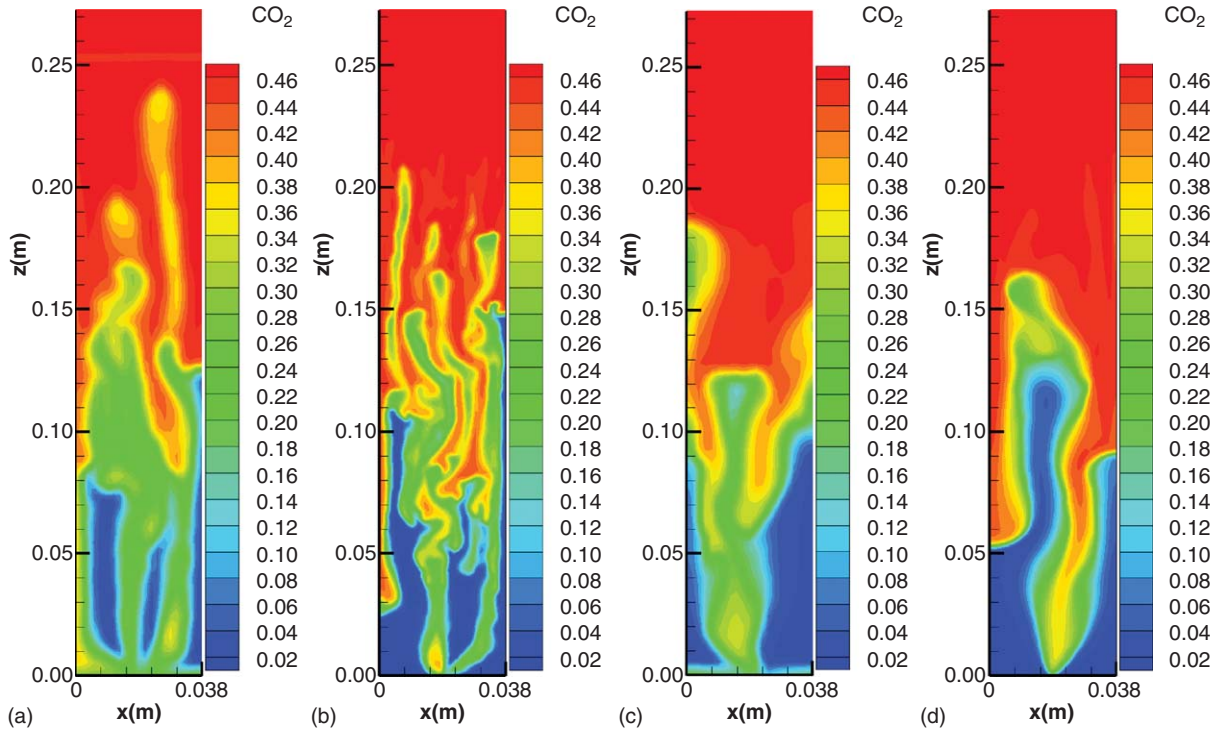

Fig. 12—DG simulations of Experiment 2: Overall CO_2 composition (molar fraction) at 0.67 PVI without Fickian diffusion on (a) 20×100 and (b) 50×250 meshes, and with diffusion on (c) 20×100 and (d) 50×250 meshes.

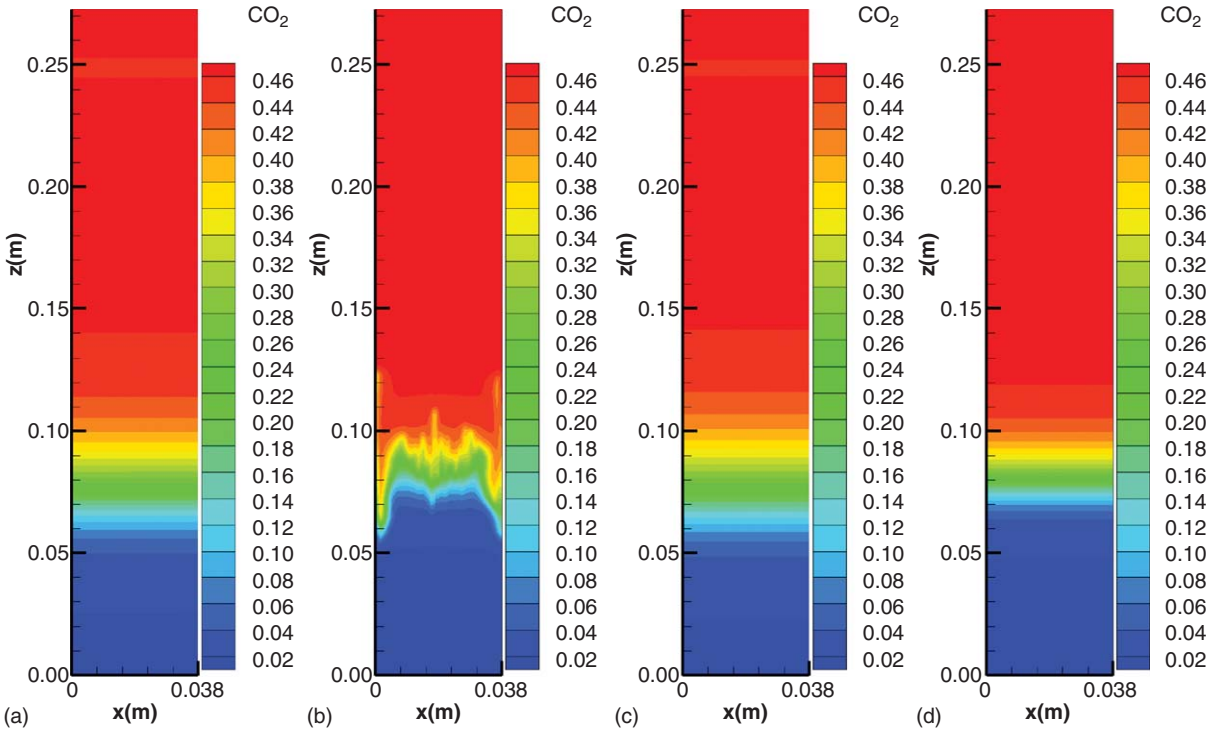

Fig. 13—FD simulations of Experiment 2: Overall CO_2 composition (molar fraction) at 0.67 PVI without Fickian diffusion on (a) 20×100 and (b) 50×250 meshes and with diffusion on (c) 20×100 and (d) 50×250 meshes.

the fingering somewhat, resulting in fewer and larger fingers, but, because of the small diffusion coefficients in the near-critical region, the stabilizing effect is insufficient to improve recovery.

The consequence of the gravitational instability manifests itself in the recovery data in Fig. 6 by the early breakthrough and low final recovery of 84% owing to the high GOR. The CO_2 and C_1 composition profiles in the gas phase (Figs. 6c and 6d) show fluctuations when different gravitational fingers reach the production well—many small ones when diffusion is neglected, and a few larger ones in simulations with diffusion. The time intervals at which experimental data on compositions in the production well are taken cannot provide conclusive evidence of the degree of fingering.

The simulations predict a slightly higher recovery than observed in the experiment. This may be expected, because the impact of gravitational fingering is more pronounced in 3D than in our 2D simulation. Nevertheless, the simulation results reproduce the measurements well.

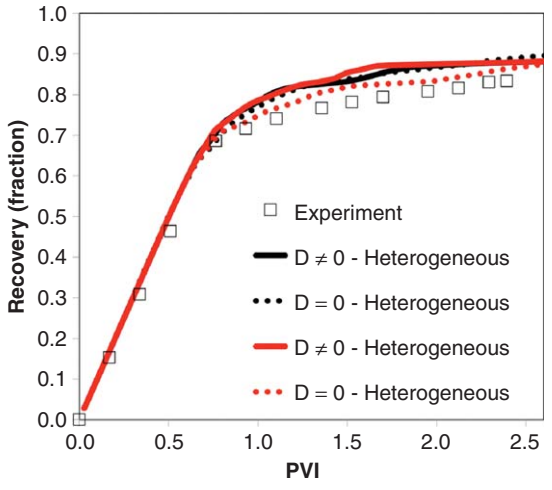

Fig. 14—DG simulations of Experiment 2: Dependence of oil recovery on ±2.5% core heterogeneity, computed on 20×100 mesh with Fickian diffusion.

Clearly, in this experiment, the onset and further development of the gravitational instability is critical. As was mentioned in the discussion of the previous experiment, numerical dispersion artificially suppresses the gravitational fingering. In **Fig. 13,** we see that for simulations on both Grid 1 and Grid 2, using a lower-order FD mass transport update, no gravitational fingers have developed, even when Fickian diffusion is neglected. As a result, the FD simulations do not predict the correct breakthrough time, and overestimate the recovery until the CO_2 front reaches the bottom of the core. We like to point out that with a first-order FD approach, one may not be able to capture fingers without going to very fine gridding, which may not be practical because of the high demand in CPU time. In two focused studies, Stalkup (1990) and Stalkup et al. (1990) did not achieve convergence with grid refinement using FD methods, and concluded that a practical approach may require extrapolation to zero grid sizes. We do not see such a need in our finite-element approach.

In heterogeneous reservoirs, gravitational instabilities may play an even more important role. In the context of oil recovery, fingering may lead to early breakthrough, while in carbon-sequestration studies, the gravitationally induced natural convection is beneficial, because it mixes injected CO_2 with water at a higher rate than through diffusion alone. Numerical dispersion, inherent to lower-order methods, may be a serious limitation in the modeling of such problems. Finer meshes may reduce the numerical dispersion, but incur high CPU costs. We also note here that in our modeling, the FD approximation is only applied to the mass-transport update. The fluxes are still updated using the MHFE method, which is more accurate than a traditional FD approach.

We further investigate the importance of core heterogeneity and relative permeability in this experiment (on Grid 1). In **Fig. 14,** we find that small variations in the core permeability result in slightly lower recovery, closer to the measured data, when diffusion is neglected. The heterogeneity provides a trigger for the first onset of gravitational fingering. However, even weak Fickian diffusion dampens this effect and renders the oil recovery insensitive to small heterogeneities. We could pursue this line of investigation and consider larger, and correlated, heterogeneities, but this is not supported by our experimental data, and is beyond the scope of this work.

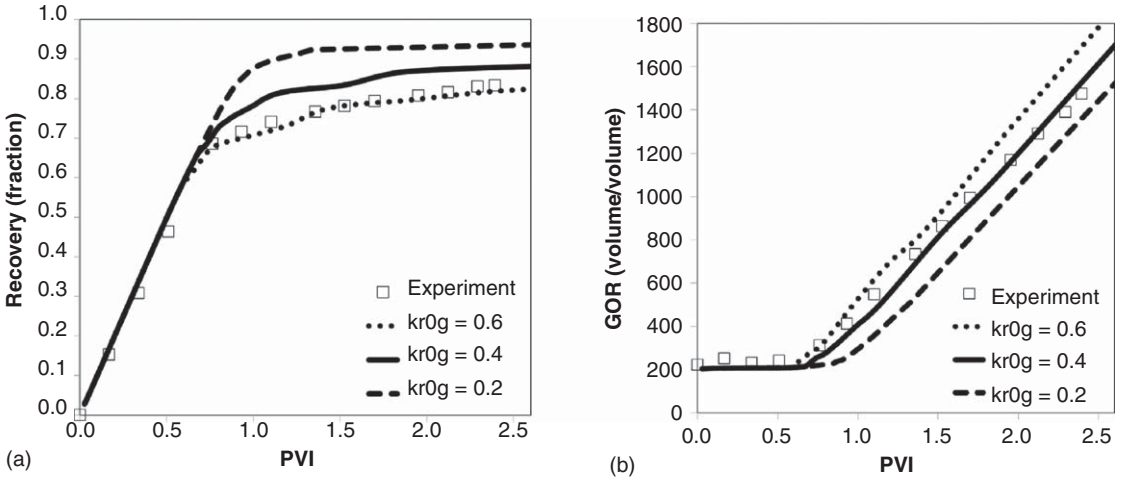

Fig. 15—DG simulations of Experiment 2: Dependence of (a) oil recovery and (b) GOR on gas relative permeability endpoint, computed on 20×100 mesh with Fickian diffusion.

The sensitivity of the results to relative permeability depends most strongly on the endpoint gas relative permeability, similar to the discussion for Experiment 1. This is illustrated in **Fig. 15** for oil recovery and GOR for simulations on Grid 1 with Fickian diffusion (the results without Fickian diffusion are similar). We find that a higher endpoint gas relative permeability results in a lower recovery, closer to the measured data. The higher gas mobility results in gravitational fingers breaking through at an earlier time. However, we also see that the higher gas mobility results in an overprediction of GOR. Furthermore, from Fig. 11, we note that an endpoint gas relative permeability of 0.6 significantly underpredicts the oil recovery for Experiment 1. We therefore conclude that the endpoint relative permeabilities of 0.6 for oil and 0.4 for gas produce the best agreement with the experimental data.

Experiment 3: CO_2 Injection From the Bottom in a Vertical Core. The most relevant and efficient CO_2 injection scenario for these conditions is to inject CO_2 from the bottom and produce oil from the top. Because the CO_2 is denser than the oil, it may essentially push out the oil in a piston-like displacement. As a result, the final recovery for this experiment is the highest at 98% (Fig. 7a). A few aspects of the phase behavior are worth mentioning.

First, the experimental data from Experiments 1 and 2 suggest that the residual oil saturation of the porous media may be up to 12%. However, as was mentioned in the Introduction, and as can be seen from the 98% recovery in Experiment 3, residual oil saturation may lose its meaning in studying CO_2 injection because of swelling and evaporation of the residual oil.

The second, related remark pertains to the evaporation of lighter oil components. At the phase boundary, methane in particular evaporates into the CO_2-rich gas phase. While pure CO_2 is denser than the oil, the CO_2/methane mixture is lighter, and flows upward faster in gravitational plumes, as illustrated in **Fig. 16.** As a result, the displacement is not quite piston-like, and both oil recovery and compositions in the production well show a more dispersed front (Fig. 7).

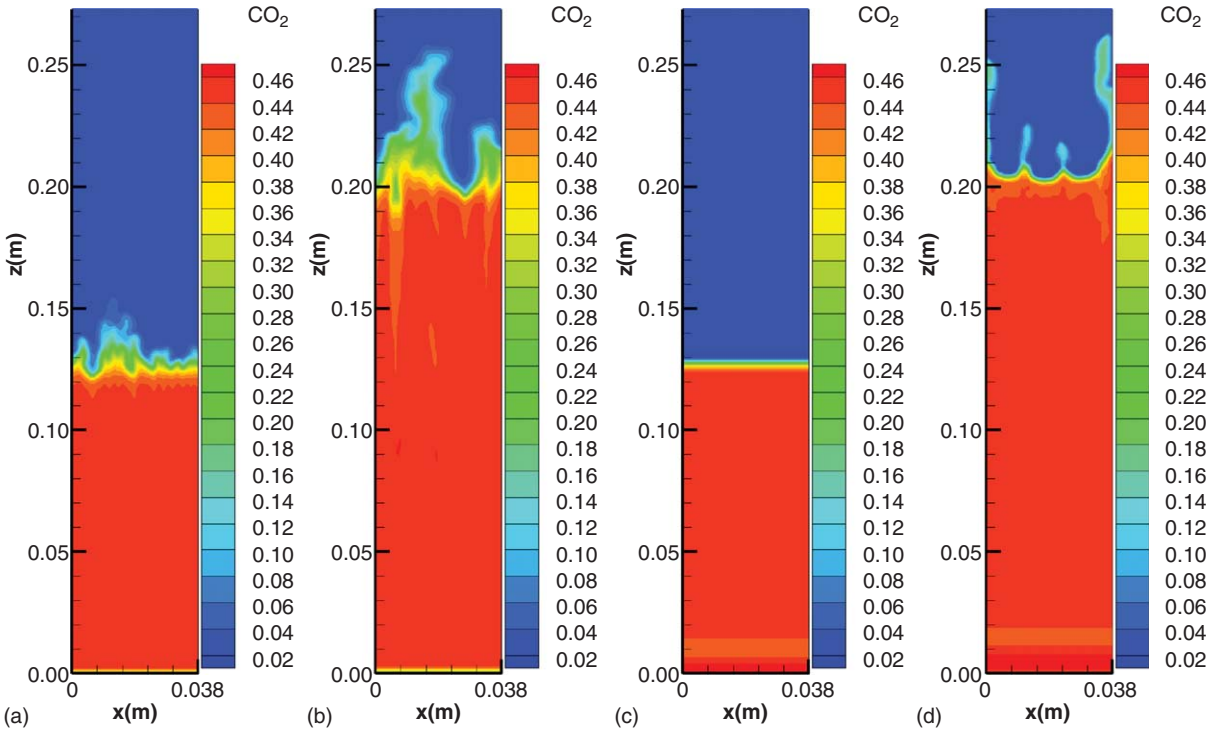

Fig. 16—DG simulations of Experiment 3: Overall CO_2 composition (molar fraction) at (a) 0.46 PVI and (b) 0.74 PVI with Fickian diffusion and at (c) 0.46 PVI and (d) 0.74 PVI without Fickian diffusion on 50×250 mesh.

The measured dispersion around the front is larger than our prediction. The reason is likely the same as for the slight overestimation of the recovery in Experiment 2: we expect the gravitational fingering caused by evaporation to be more pronounced in 3D than in our 2D modeling. Underprediction of evaporation caused by our fluid characterization seems unlikely, because we obtain nearly identical results for a range of different pseudoizations and residues up to C_{30+}.

Despite this limitation, the simulations predict the correct final recovery and agree reasonably well on the measured GOR and compositional profiles. Simulations for a heterogeneous domain, in which the permeability is randomly perturbed throughout the domain by $\pm 2.5\%$, predict nearly identical results (not shown). The simulations for this experiment are also insensitive to relative permeability. This is to be expected for near-piston-like displacement of oil by gas.

Generally speaking, we can reproduce and understand the main features of all three experiments carried out in this work.

Effect of Connate Water. Our higher-order compositional simulator accurately models the solubility of CO_2 in the connate water and the phase behavior of the resulting CO_2/water mixture. The CO_2 solubility is obtained from the requirement of equal fugacity of CO_2 in the oil, water, and gas phases. The phase behavior of the CO_2/water mixture is modeled using a cubic-plus-association and cross-association equation of state. At the experimental conditions, the maximum CO_2 solubility in water is 2.8 mol%, or 6.8 mass%. We assumed a water viscosity of 0.48 cp and linear water relative permeability with endpoint 0.3.

The dissolution of CO_2 reduces the sweep of the hydrocarbon volume. However, a competing effect is the swelling by up to 5.2 vol% of the aqueous phase due to CO_2 dissolution. At the same time, CO_2 has a high solubility in the oil, and from Fig. 4b, we find that the swelling of the oil phase may be up to 20 vol%. The net effect of the aforementioned processes is that in all three experiments, the recovery rate before breakthrough is slightly superlinear.

A related effect is that the swelling of the aqueous phase increases the water saturation above the residual (connate) level of 31.14% and allows a small amount of water to flow. The density of the mobile water (0.999 g/cm^3) is higher than that of the oil and of CO_2. The water therefore tends to drain to the bottom, which results in a total water recovery of less than 0.1 vol% in Experiments 1 and 3. In Experiment 2, any nonzero water mobility may amplify the gravitational instability: when CO_2 is injected from the top and swells the oil above the residual saturation, both dense CO_2 and dense mobile water sit on top of lighter oil. In the subsequent natural convection, some of the mobile water flows downward and reaches the outlet. No water production was measured in the experiments, but the simulations predict a total water production for Experiment 2 of approximately 2.5 vol%. In summary, the presence of connate water has little effect on the experiments, and simulations in which the connate water is simply treated as a porosity reduction provide similar results.

Conclusions

The main conclusions drawn from this work are:

1. **Endpoint relative permeability.** The simulation results are sensitive to the endpoint relative permeability of the gas phase, but not to the exponents or the endpoint relative permeability of the oil phase. The measurements can only be reproduced with low endpoints for the gas phase of 0.3–0.4. These values may be similar or even lower than for the oil phase. Given that the gas and oil phase viscosities are similar in the near-critical region, the phase mobilities are also similar, and the distinction between intermediate wetting and non-wetting phases may not be significant.
2. **Effect of gravity.** The unique properties of CO_2 deserve careful consideration, as compared with, for instance, N_2 injection. In particular, CO_2 is supercritical at the temperatures and pressures pertaining to a number of reservoirs, and the density of CO_2 may be higher than the density of the reservoir oil. Consequently, CO_2 injection from the top is gravitationally unstable and generally results in fingering and subsequent fast natural convection. The latter may efficiently mix the CO_2 throughout the domain, but results in early breakthrough and low recovery. We would like to emphasize that these findings could not be obtained from a slim-tube experiment. Various effects that are essential in understanding CO_2 injection in a gravitational domain, and where diffusion is important, cannot be modeled in one dimension.
3. **Effect of diffusion.** We have seen that the higher-order modeling of the gravitationally unstable Experiment 2 results in the nearly instantaneous development of gravitational fingers, followed by fast convection when Fickian diffusion is not accounted for. When diffusion is strong, it would dampen the instability and result in higher recovery. In these experiments, the fluid is in the near-critical region, where we observe a need for substantially reduced diffusion coefficients. This analysis provides further support for this notion. The measured data can be reproduced most accurately when Fickian diffusion is incorporated in the modeling, but with diffusion coefficients that are reduced by an overall factor of ≤ 0.01 with respect to the coefficients in open-space diffusion, far from the critical point.
4. **Need for higher-order methods.** The numerical dispersion inherent to the use of lower-order methods may in some cases mimic some of the features of Fickian diffusion, but has no physical basis and may in fact obscure essential processes. In particular, with a FD approximation, we cannot reproduce the experimental results and DG simulations for the gravitationally unstable second experiment, even on a very fine mesh. To achieve the same accuracy using a FD method, one would have to repeat the discussed simulations on an even finer mesh, and at a correspondingly higher computational (CPU) cost. Similarly, FD methods may not provide the high accuracy in the calculation of the convective fluxes that we obtain by using the MHFE method. This accuracy for fluxes is important to reliably predict the complicated velocity field associated with the observed natural convection.

Acknowledgments

We would like to thank Intertek Westport Technology Center, Houston, for carrying out the experiments. We would also like to thank Petrobras for permission to publish this work, which was supported by member companies of RERI.

References

Ashcroft, S.J. and Isa, M.B. 1997. Effect of Dissolved Gases on the Densities of Hydrocarbons. *J. Chem. Eng. Data* **42** (6): 1244–1248. http://dx.doi.org/10.1021/je9701588.

Brigham, W.E., Reed, P.W., and Dew, J.N. 1961. Experiments on Mixing During Miscible Displacement in Porous Media. *SPE J.* **1** (1): 1–8. SPE-1430-G. http://dx.doi.org/10.2118/1430-G.

Cavett, R.H. 1962. Physical Data for Distillation Calculation, Vapor-Liquid Equilibria. *Proc.*, Midyear Meeting of the 27th API Division of Refining, San Francisco, 15 May, Vol. 52, 351–354.

Christensen, P.L. and Pedersen, K.S. 1962. *Phase Behavior of Petroleum Reservoir Fluids*. Boca Raton, Florida: CRC Press.

Cussler, E.L. 1997. *Diffusion: Mass Transfer in Fluid Systems*, second edition. Cambridge, UK: Cambridge Series in Chemical Engineering, Cambridge University Press.

DOE Fossil Energy Office of Communications. 2011. Fossil Energy: DOE's Oil Recovery R&D Program, http://fossil.energy.gov/programs/oilgas/eor/ (accessed 2008).

Donaldson, E.C., Kendall, R.F., and Manning, F.S. 1976. Dispersion and Tortuosity in Sandstones. Paper SPE 6190 presented at the SPE Annual Fall Technical Conference and Exhibition, New Orleans, 3–6 October. http://dx.doi.org/10.2118/6190-MS.

Firoozabadi, A. 1999. *Thermodynamics of Hydrocarbon Reservoirs.* New York: McGraw-Hill.

Firoozabadi, A., Katz, D.L., Soroosh, H. et al. 1988. Surface Tension of Reservoir CrudeOil/Gas Systems Recognizing the Asphalt in the Heavy Fraction. *SPE Res Eng* **3** (1): 265–272. SPE-13826-PA. http://dx.doi.org/10.2118/13826-PA.

Ghorayeb, K. and Firoozabadi, A. 2000. Molecular, pressure, and thermal diffusion in nonideal multicomponent mixtures. *AIChE J.* **46** (5): 883–891. http://dx.doi.org/10.1002/aic.690460503.

Hoteit, H. and Firoozabadi, A. 2005. Multicomponent fluid flows by discontinuous Galerkin and mixed methods in unfractured and fractured media. *Water Resour. Res.* **41** (W11412): 1–15. http://dx.doi.org/10.1029/2005WR004339.

Hoteit, H. and Firoozabadi, A. 2006a. Compositional Modeling by the Combined Discontinuous Galerkin and Mixed Methods. *SPE J.* **11** (1): 19–34. SPE-90276-PA. http://dx.doi.org/10.2118/90276-PA.

Hoteit, H. and Firoozabadi, A. 2006b. Compositional Modeling of Discrete-Fractured Media Without Transfer Functions by the Discontinuous Galerkin and Mixed Methods. *SPE J.* **11** (3): 341–352. SPE-90277-PA. http://dx.doi.org/10.2118/90277-PA.

Hoteit, H. and Firoozabadi, A. 2009. Numerical Modeling of Diffusion in Fractured Media for Gas Injection and Recycling Schemes. *SPE J.* **14** (2): 323–337. SPE-103292-PA. http://dx.doi.org/ 10.2118/103292-PA.

Jhaveri, B.S. and Youngren, G.K. 1988. Three-Parameter Modification of the Peng-Robinson Equation of State To Improve Volumetric Predictions. *SPE Res Eng* **3** (3): 1033–1040. SPE-13118-PA. http://dx.doi.org/10.2118/13118-PA.

Leahy-Dios, A. and Firoozabadi, A. 2007. Unified model for nonideal multicomponent molecular diffusion coefficients. *AIChE J.* **53** (11): 2932–2939. http://dx.doi.org/10.1002/aic.11279.

Li, Z. and Firoozabadi, A. 2012. General Strategy for Stability Testing and Phase-split Calculations in Two and Three Phases. *SPE J.* **17** (4): 1096–1107. SPE-129844-PA. http://dx.doi.org/10.2118/129844-PA.

Lohrenz, J., Bray, B.G., and Clark, C.R. 1964. Calculating Viscosities of Reservoir Fluids From Their Compositions. *J Pet Technol* **16** (10): 1171–1176. SPE-915-PA. http://dx.doi.org/10.2118/915-PA.

Moortgat, J. and Firoozabadi, A. 2010. Higher-order compositional modeling with Fickian diffusion in unstructured and anisotropic media. *Adv. Water Resour.* **33** (9): 951–968. http://dx.doi.org/10.1016/j.advwatres.2010.04.012.

Moortgat, J., Sun, S., and Firoozabadi, A. 2011. Compositional modeling of three-phase flow with gravity using higher-order finite element methods. *Water Resour. Res.* **47** (5): W05511. http://dx.doi.org/10.1029/2010wr009801.

Moortgat, J., Li, Z., and Firoozabadi, A. 2012. Three-Phase Compositional Modeling of CO_2 Injection by Higher-Order Finite Element Methods with CPA Equation of State for Aqueous Phase. *Water Resour. Res.* **48,** W12511, doi: 10.1029/2011WR011736.

Müller, N. 2011. Supercritical CO_2-Brine Relative Permeability Experiments in Reservoir Rocks—Literature Review and Recommendations. *Transport Porous Media* **87** (2): 367–383. http://dx.doi.org/10.1007/s11242-010-9689-2.

Peng, D.-Y. and Robinson, D.B. 1976. A New Two-Constant Equation of State. *Industrial & Engineering Chemistry Fundamentals* **15** (1): 59–64. http://dx.doi.org/10.1021/i160057a011.

Rongy, L., Haugen, K.B., and Firoozabadi, A. 2012 Mixing from Fickian diffusion and natural convection in binary non-equilibrium fluid phases, *AIChE J.* **58** (5): 1336-1345.

Simon, R., Rosman, A., and Zana, E. 1978. Phase-Behavior Properties of CO2–Reservoir Oil Systems. *SPE J.* **18** (1): 20-26. SPE-6387-PA. http://dx.doi.org/10.2118/6387-PA.

Stalkup, F.I. 1990. Effect of Gas Enrichment and Numerical Dispersion on Enriched-Gas-Drive Predictions. *SPE Reservoir Engineering* **5** (4): 647–655. SPE-18060-PA. http://dx.doi.org/10.2118/18060-PA.

Stalkup, F.I., Lo, L.L., and Dean, R.H. 1990. Sensitivity to Gridding of Miscible Flood Predictions Made With Upstream Differenced Simulators. Paper SPE 20178 presented at the SPE/DOE Enhanced Oil Recovery Symposium, Tulsa, 22–25 April. http://dx.doi.org/10.2118/20178-MS.

van Brakel, J. and Heertjes, P.M. 1974. Analysis of diffusion in macroporous media in terms of a porosity, a tortuosity and a constrictivity factor. *Int. J. Heat Mass Transfer* **17** (9): 1093–1103. http://dx.doi.org/10.1016/0017-9310(74)90190-2.

Appendix

In this Appendix, we provide more details of the fluid characterization and the pseudoization used in the PVT analysis and simulations of the coreflood experiments. First, a full reservoir fluid characterization was performed up to a residue of C_{30+}, as provided in **Table 1** for the coreflooding experiments. Next, various pseudoizations were constructed to reduce the number of components for efficient simulation. The optimal pseudoized characterization in terms of both accuracy and minimal number of (pseudo-) components was achieved by nine pure- and pseudocomponents: CO_2, N_2+C_1, C_2, C_3, C_4-C_5, C_6-C_9, C_{10}-C_{14}, C_{15}-C_{19}, and C_{20+}. Figs. 1 through 4 compare the experimental data to predictions using this pseudoization, as well as computed results with 7, 8, 10, and 11 component pseudoizations with a residue of C_{30+}. The latter four pseudoizations are CO_2, N_2+C_1, C_2-C_4, C_5-C_{10}, C_{11}-C_{19}, C_{20}-C_{29}, C_{30+}; CO_2, N_2+C_1, C_2-C_4, C_5-C_9, C_{10}-C_{16}, C_{17}-C_{23}, C_{24}-C_{29}, C_{30+}; CO_2, N_2+C_1, C_2-C_3, C_4-C_5, C_6-C_9, C_{10}-C_{14}, C_{15}-C_{19}, C_{20}-C_{24}, C_{25}-C_{29}, C_{30+}; and CO_2, N_2+C_1, C_2, C_3, C_4-C_5, C_6-C_9, C_{10}-C_{14}, C_{15}-C_{19}, C_{20}-C_{24}, C_{25}-C_{29}, C_{30+}. The matching procedure is the same as described in the following.

TABLE 1—COMPOSITION (MOLE FRACTION) *Z*, MOLECULAR WEIGHT M_W, CRITICAL TEMPERATURE T_C, CRITICAL PRESSURE P_C, ACENTRIC FACTOR Ω, AND VOLUME SHIFT PARAMETER *VSP* IN FULL FLUID CHARACTERIZATION FOR COREFLOODS

Component	z	M_W (g/mol)	T_C (K)	P_C (bar)	ω	*VSP*
CO_2	0.0840	44	304.14	73.75	0.239	−0.055
N_2	0.0045	28	126.21	33.90	0.039	−0.289
C_1	0.5037	16	190.56	45.99	0.011	−0.154
C_2	0.0684	30	305.32	48.72	0.099	−0.100
C_3	0.0432	44	369.83	42.48	0.153	−0.085
iC_4	0.0092	58	407.80	36.04	0.183	−0.079
nC_4	0.0145	58	425.12	37.96	0.199	−0.064
iC_5	0.0061	72	460.40	33.80	0.227	−0.044
nC_5	0.0090	72	469.70	33.70	0.251	−0.042
C_6	0.0126	86	507.40	30.12	0.296	−0.015
C_7	0.0201	100	556.48	26.75	0.294	0.025
C_8	0.0217	114	574.76	25.24	0.418	0.048
C_9	0.0171	128	593.07	23.30	0.491	0.068
C_{10}	0.0148	142	617.07	21.55	0.534	0.085
C_{11}	0.0127	156	638.24	19.74	0.566	0.101
C_{12}	0.0112	170	657.29	18.31	0.602	0.115
C_{13}	0.0118	184	675.70	16.96	0.639	0.127
C_{14}	0.0103	198	691.48	15.75	0.667	0.139
C_{15}	0.0091	212	707.29	14.72	0.670	0.150
C_{16}	0.0073	226	722.96	13.79	0.668	0.159
C_{17}	0.0068	240	738.12	12.98	0.670	0.169
C_{18}	0.0069	254	749.81	12.31	0.696	0.177
C_{19}	0.0062	268	761.50	11.68	0.705	0.185
C_{20}	0.0063	282	780.91	11.07	0.707	0.193
C_{21}	0.0054	296	792.72	10.57	0.750	0.200
C_{22}	0.0053	310	803.27	10.12	0.782	0.207
C_{23}	0.0050	324	813.48	9.71	0.808	0.213
C_{24}	0.0042	338	822.92	9.33	0.834	0.219
C_{25}	0.0043	352	831.76	9.01	0.889	0.225
C_{26}	0.0039	366	840.59	8.68	0.977	0.230
C_{27}	0.0037	380	849.11	8.40	1.003	0.235
C_{28}	0.0035	394	857.47	8.14	1.076	0.240
C_{29}	0.0039	408	865.83	7.95	1.182	0.245
C_{30+}	0.0433	803	1009.72	7.00	1.580	0.321

Table 2 lists the composition of the reservoir fluid up to C_{20+}, used in the PVT measurements of differential liberation. The residue C_{20+} is represented by its molecular weight (536 g/mol) and specific gravity (0.9594). The pseudoization is based on the amount and volatility range of the pure components. The critical temperature T_C, critical pressure P_C, acentric factor ω, molecular weight M_W, and volume shift parameter *VSP* of pure components

TABLE 2—COMPOSITION OF RESERVOIR FLUID IN THE PVT EXPERIMENT

Component	Mole Fraction	Component	Mole Fraction
CO_2	0.0824	C_9	0.0169
N_2	0.0037	C_{10}	0.0155
C_1	0.5129	C_{11}	0.0126
C_2	0.0707	C_{12}	0.0115
C_3	0.0487	C_{13}	0.0119
iC_4	0.0090	C_{14}	0.0098
nC_4	0.0179	C_{15}	0.0096
iC_5	0.0059	C_{16}	0.0075
nC_5	0.0086	C_{17}	0.0068
C_6	0.0113	C_{18}	0.0069
C_7	0.0164	C_{19}	0.0063
C_8	0.0210	C_{20+}	0.0762

TABLE 3—COMPOSITION (MOLE FRACTION) *Z*, MOLECULAR WEIGHT M_W, CRITICAL TEMPERATURE T_C, CRITICAL PRESSURE P_C, ACENTRIC FACTOR Ω, AND VOLUME SHIFT PARAMETER *VSP* IN THE FLUID CHARACTERIZATION OF PVT EXPERIMENTS

Component	*z*	M_W (g/mol)	T_C (K)	P_C (bar)	ω	*VSP*
CO_2	0.0824	44	304.14	73.75	0.239	−0.055
N_2+C_1	0.5166	16	190.10	45.90	0.011	−0.155
C_2	0.0707	30	305.32	48.72	0.099	−0.100
C_3	0.0487	44	369.83	42.48	0.153	−0.085
C_4-C_5	0.0414	63	435.64	36.06	0.210	−0.060
C_6-C_9	0.0656	109	563.30	25.96	0.385	0.036
C_{10}-C_{14}	0.0613	167	652.24	18.75	0.595	0.111
C_{15}-C_{19}	0.0371	237	733.22	13.25	0.680	0.166
C_{20+}	0.0762	536	907.90	7.98	1.477	0.308

TABLE 4—NONZERO BINARY INTERACTION COEFFICIENTS (BICs)

	N_2+C_1	C_2	C_3	C_4-C_5	C_6-C_9	C_{10}-C_{14}	C_{15}-C_{19}	C_{20+}
CO_2	0.130	0.130	0.130	0.130	0.130	0.130	0.130	0.130
N_2+C_1		0.034	0.036	0.039	0.047	0.056	0.068	0.116

TABLE 5—COMPOSITION OF THE RESERVOIR FLUID IN THE COREFLOODING EXPERIMENTS

Component	Mole Fraction	Component	Mole Fraction
CO_2	0.0840	C_9	0.0171
N_2	0.0045	C_{10}	0.0148
C_1	0.5034	C_{11}	0.0127
C_2	0.0684	C_{12}	0.0112
C_3	0.0432	C_{13}	0.0118
iC_4	0.0092	C_{14}	0.0103
nC_4	0.0145	C_{15}	0.0091
iC_5	0.0061	C_{16}	0.0073
nC_5	0.0090	C_{17}	0.0068
C_6	0.0126	C_{18}	0.0069
C_7	0.0201	C_{19}	0.0062
C_8	0.0217	C_{20+}	0.0889

(CO_2, N_2, C_1, C_2, C_3, iC_4, nC_4, iC_5, and nC_5), and pseudo-hydrocarbon components ($C_6 \sim C_{19}$) are directly available (Firoozabadi 1999). For the pseudocomponents N_2+C_1, C_4-C_5, C_6-C_9, C_{10}-C_{14}, and C_{15}-C_{19}, we take the molar average to obtain T_C, P_C, ω, M_W, and *VSP*, while for C_{20+}, Cavett's correlation (Cavett 1962) is applied to estimate T_C, based on the molecular weight and specific gravity.

The binary interaction coefficients (BICs, K_{IJ}) between N_2+C_1 and other components (except CO_2) are calculated by (Firoozabadi 1999): $K_{2j} = 0.0289 + 1.633\text{E-}4 \times \text{Mw}\ (C_j)$. The BICs between CO_2 and other components are assumed identical. We are left with three adjustable parameters to match the bubblepoint pressures of the reservoir fluid and its mixtures with CO_2 in the PVT experiments at 331.85 K: the CO_2-related BICs, and P_C and ω of C_{20+}. The *VSP* of CO_2 is tuned to match the density of pure CO_2 (0.916 g/cm^3) at reservoir conditions (331.2 K and 441.3 bar). The *VSP* of C_{20+} is adjusted to match the oil density in the PVT experiments at 331.85 K and various pressures. The EOS parameters are provided in **Tables 3 and 4.** It should be noted that the composition of the reservoir fluid in the coreflooding experiments **(Table 5)** is slightly different from those in the PVT experiments. The corresponding mole-weighed T_C, P_C, ω, M_W, and *VSP* are listed in **Table 6.** We use the BICs in Table 4, because the M_W of pseudocomponents is nearly the same.

Joachim Moortgat is a postdoctoral researcher at RERI. email: jmoortgat@rerinst.org. His research interests are in the theory and advanced numerical modeling of compositional multiphase flow in subsurface fractured porous media. He holds MS degrees in theoretical physics and astrophysics, both from

TABLE 6—FLUID CHARACTERIZATION (AS IN TABLE 3) FOR THE COREFLOODING EXPERIMENTS

Component	*z*	M_W (g/mol)	T_C (K)	P_C (bar)	ω	*VSP*
CO_2	0.0840	44	304.14	73.75	0.239	−0.055
N_2+C_1	0.5080	16	189.99	45.88	0.011	−0.155
C_2	0.0684	30	305.32	48.72	0.099	−0.100
C_3	0.0432	44	369.83	42.48	0.153	−0.085
C_4-C_5	0.0388	64	436.89	35.86	0.212	−0.059
C_6-C_9	0.0715	109	562.11	26.06	0.379	0.035
C_{10}-C_{14}	0.0609	168	652.92	18.70	0.596	0.111
C_{15}-C_{19}	0.0363	238	733.59	13.23	0.681	0.166
C_{20+}	0.0889	536	907.90	7.98	1.477	0.308

Utrecht University, the Netherlands, and a PhD degree in astrophysics from the Radboud University, the Netherlands.

Abbas Firoozabadi is the senior scientist and director at RERI. He also teaches at Yale University. email: af@rerinst.org. His main research activities center on thermodynamics of hydrocarbon reservoirs and production and on multiphase-multicomponent flow in fractured petroleum reservoirs. Firoozabadi holds a BS degree from the Abadan Institute of Technology, Abadan, Iran, and MS and PhD degrees from the Illinois Institute of Technology, Chicago, all in gas engineering. Firoozabadi is the recipient of the 2002 SPE/AIME Anthony Lucas Gold Medal and is a member of the National Academy of Engineering.

Zhidong Li is a postdoctoral researcher at RERI. email: zli@rerinst.org. His research interest is in thermodynamics of IOR/EOR with gas/water injection, asphaltene precipitation and stabilization, shale gas/oil, multiphase equilibrium computation, and PVT modeling. Li holds BS and MS degrees from Tsinghua University, Beijing, China, and a PhD degree from the University of California at Riverside, all in chemical engineering.

Rogério Espósito is a process engineer at Petrobras SA, Brazil. His main research covers thermodynamic modeling of reservoir fluids and phase/chemical equilibrium in porous media. He holds BS, MS, and PhD degrees in chemical engineering from the Federal University of Rio de Janeiro.